First-principles anisotropic constitutive relationships in β-cyclotetramethylene tetranitramine (β-HMX)

M. W. Conroy,[1,a] I. I. Oleynik,[1] S. V. Zybin,[2] and C. T. White[3]
[1]*Department of Physics, University of South Florida, Tampa, Florida 33620, USA*
[2]*Materials and Process Simulation Center, California Institute of Technology, Pasadena, California 91125, USA*
[3]*Naval Research Laboratory, Washington, DC 20375, USA*

(Received 14 May 2008; accepted 26 June 2008; published online 5 September 2008)

First-principles density functional theory calculations have been performed to obtain constitutive relationships in the crystalline energetic material β-cyclotetramethylene tetranitramine (β-HMX). In addition to hydrostatic loading, uniaxial compressions in the directions normal to the {100}, {010}, {001}, {110}, {101}, {011}, and {111} planes have been performed to investigate the anisotropic equation of state (EOS). The calculated lattice parameters and hydrostatic EOS are in reasonable agreement with the available experimental data. The uniaxial compression data show a significant anisotropy in the principal stresses, change in energy, band gap, and shear stresses, which might lead to the anisotropy of the elastic-plastic shock transition and shock sensitivity of β-HMX. © *2008 American Institute of Physics*. [DOI: 10.1063/1.2973689]

I. INTRODUCTION

Cyclotetramethylene tetranitramine or 1,3,5,7-tetranitro-1,3,5,7-tetraazacyclooctane, also known as HMX, is an important energetic material (EM) used in many explosive applications. The HMX molecular crystal exists in several crystallographic polymorphs, α, β, δ, ε, and ϕ, the β phase being the ground state structure at ambient conditions.[1,2] Because of its widespread applications including plastic bonded explosive formulations, HMX has been extensively studied both experimentally and theoretically. In particular, several groups have investigated the physical behavior of HMX under hydrostatic compression. Yoo and Cynn[2] have performed hydrostatic and nonhydrostatic compression experiments on β-HMX using a diamond anvil cell. The x-ray diffraction and micro-Raman spectroscopy results indicate phase transitions under hydrostatic compression to the ε and ϕ polymorphs at 12 and 27 GPa, respectively.[2] Gump and Peiris[3] have also performed both hydrostatic and nonhydrostatic compression of β-HMX at temperatures of 30, 100, and 140 °C and at pressures below 5.8 GPa. In their experiments, HMX remained in the β phase at all temperatures up to 5.8 GPa, but their samples were converted to the δ phase upon decompression.[3]

In addition to experimental work, several theoretical investigations of the hydrostatic compression of HMX have also been performed. Sewell[4] used a rigid molecule approximation and classical intermolecular potentials (force fields) parametrized for near-ambient conditions to perform Monte Carlo simulations of hydrostatic compression of the β phase up to pressures of 7.5 GPa. Similar calculations employing force-field based isothermal-isobaric molecular dynamics (MD) and molecular packing have been done by Sorescu *et al.*[5] Later, Sewell *et al.*[6] performed MD calculations to simulate the compression of the pure polymorphs of HMX (α, β, and δ) and obtained room-temperature isotherms and elastic constants, including bulk and shear moduli, for each of the phases. In addition to classical force-field based Monte Carlo methods and MD, density functional theory (DFT) calculations of HMX have also been completed.[7–10] Byrd *et al.*[7] calculated the structure of HMX and other EMs at zero pressure with various DFT functionals. They attributed the overestimation of unit-cell volume to the poor description of van der Waals interactions by DFT. Later, Byrd and Rice[8] performed DFT calculations of hydrostatic compression of β-HMX among other EMs and showed that as compression increases, the DFT results display better agreement with experiment due to a greater overlap of electronic densities. Recently, two studies have employed the local-density approximation of DFT to examine the electronic structure and vibrational frequencies of the α, β, γ, and δ polymorphs of HMX (Ref. 9) and the hydrostatic compression of the β polymorph.[10] Similar to DFT, the Hartree–Fock calculations of hydrostatic compression performed by Zerilli and Kuklja[11] have yielded results in agreement with experiment.

Although the hydrostatic compression of HMX provides valuable information on mechanical and thermodynamical properties of this material, the understanding of fundamental physics and chemistry of detonation, including its shock initiation, requires a detailed knowledge of material's response beyond hydrostatic loading. Shock wave propagation in the material involves rapid uniaxial compressions. Such mechanical load creates shear stresses, which are the driving forces of the plastic deformations in the material. Therefore, the extension of the hydrostatic equation of state (EOS) of HMX to include the anisotropic constitutive relationships is one of the urgent needs of the EM research community.

Several studies on shock compression of HMX have already been done. In particular, Dick *et al.*[12] performed plane shock wave experiments on β-HMX for the {110}, {011}, and {010} orientations of the $P2_1/n$ space group and found greater elastic precursor strengths for the {010} shocks. In

[a]Electronic mail: mconroy@shell.cas.usf.edu.

TABLE I. Calculated zero-pressure lattice constants and volume of β-HMX compared with the experimental data at ambient conditions.

Work	a (Å)	b (Å)	c (Å)	β	V (Å^3)
Reference 30	6.54	11.05	8.702	124.325°	519.372
Reference 31	6.54	11.05	8.7	124.3°	519.387
This work	6.70(+2.4%)	11.35(+2.7%)	8.91(+2.4%)	124.13°(−0.2°)	560.81(+8.0%)

their previous experiments on pentaerythritol tetranitrate (PETN),[13,14] a correlation between higher sensitivity and greater elastic precursor strength has been found. To extend this correlation to the case of HMX, Menikoff *et al.*[15] performed a modeling of these experiments using a rate-dependent elastic-plastic model. Further, Hare *et al.*[16] and Hooks *et al.*[17] have conducted isentropic compression experiments on HMX to determine if the phase transitions proposed by Yoo and Cynn[2] take place on time scales corresponding to shock-loading conditions, and no transitions have been observed. Rae *et al.*[18] investigated the quasistatic compressive stress versus strain in a single crystal β-HMX and found an elastic-plastic response in the case of uniaxial compression applied on the (110) face. Hooks and Ramos[19] also found that contrary to the assumption of a correlation between greater elastic precursor strength and higher sensitivity proposed by Dick and Ritchie,[13] the onset of shock-induced reactions occurred at about the same pressure for shocks delivered in the (011) and (010) orientations.

The major goal of the current study is to systematically investigate the anisotropic response of β-HMX upon uniaxial compression along various crystallographic directions. We have already performed a similar study for another EM molecular crystal, PETN, and found a substantial degree of anisotropy in the mechanical properties of the molecular crystal.[20] By extending the hydrostatic EOS to include anisotropic material response, we would like to investigate the role of the shear stresses and possibly to correlate their behavior in the course of uniaxial compression to shock sensitivities along different crystallographic directions.

II. COMPUTATIONAL DETAILS

We apply first-principles DFT (Ref. 21) as implemented in the Vienna *ab initio* simulation package (VASP) (Refs. 22 and 23) to obtain accurate properties of β-HMX at equilibrium conditions as well as under hydrostatic and uniaxial compression. In the previous work on PETN,[20] we conducted extensive tests in order to find the calculation parameters including exchange-correlation functional, pseudopotential, energy cutoff, and k-point set that ensured accurate results. Therefore, in the present study, we used this information and performed calculations with the Perdew–Burke–Ernzerhof (PBE) (Refs. 24 and 25) functional, the projector-augmented wave (PAW) (Refs. 26 and 27) potentials, and an energy cutoff of 700 eV. Note that the cutoff energy chosen, 700 eV, is almost twice the nominal cutoff (400 eV) for the PAW potentials, and this is typically required to achieve adequate convergence for molecular crystals. The k-point set chosen for each compression is the Monkhorst–Pack[28] grid that corresponds to an average k-point spacing of 0.08 Å^{-1} in each direction when the experimental structure is compressed to half of its original volume in a manner consistent with the compression to be studied. For example, the k-point set for hydrostatic compression (and relaxation of the experimental structure) was determined by scaling the magnitude of the lattice vectors of the experimental structure by $0.5^{1/3}$, then calculating the appropriate grid for our desired k spacing. This method provides sufficiently accurate k-point sampling density as the Brillouin zone enlarges during compression. Using these settings for the DFT calculations, we obtained convergence better than 0.4 GPa in pressure, 0.0015 eV/atom in energy, and 0.015 eV/Å in forces.

We obtained the theoretical zero-pressure cell parameters of HMX by relaxing the experimental structure (space group $P2_1/c$) using the quasi-Newton structure minimization method within VASP. The relaxation allowed simultaneous optimization of the atomic coordinates and the unit-cell volume and shape without any symmetry constraints. During each step of the ionic relaxation, the energy tolerance was 10^{-6} eV. The relaxation process stopped once the maximum force on any atom was less than 0.03 eV/Å.

For the hydrostatic-compression calculations, we compressed the unit cell of HMX from $V/V_0=1.00-0.60$ in increments of 0.02. Each time the volume was scaled down, we fixed the unit-cell volume and relaxed the unit-cell shape and the atomic coordinates without a constraint on symmetry until the maximum force on any atom was less than 0.03 eV/Å.

We performed uniaxial compressions along seven plane normals: ⟨100⟩, ⟨010⟩, ⟨001⟩, ⟨110⟩, ⟨101⟩, ⟨011⟩, and ⟨111⟩.

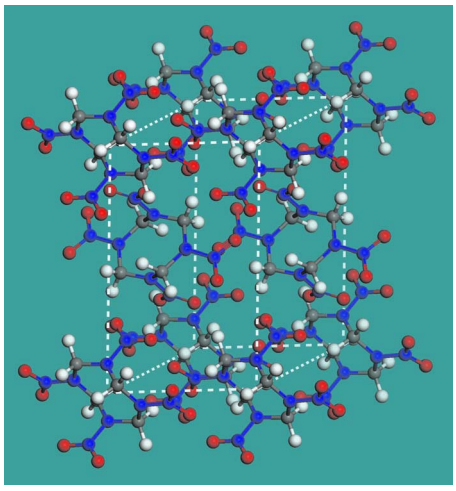

FIG. 1. (Color online) Unit cell of β-HMX.

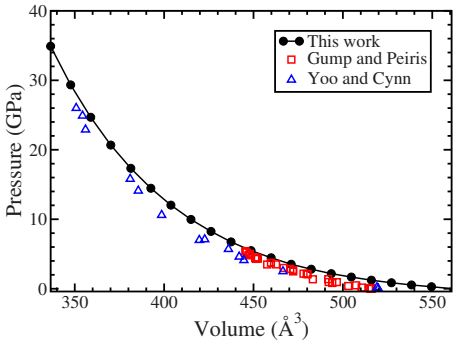

FIG. 2. (Color online) Isothermal hydrostatic EOS of β-HMX. The interval of volume shown is from 60% to 100% of the calculated zero-pressure volume.

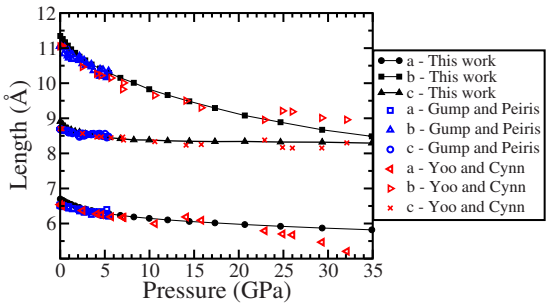

FIG. 3. (Color online) Lattice parameters of β-HMX under hydrostatic compression.

Note that the direction specified by $\langle hkl \rangle$, following the work of Dick *et al.*,[29] is perpendicular to the Miller plane $\{hkl\}$. To perform the compressions, we rotated the Cartesian coordinate system such that the x direction corresponded to the compression direction. Then, the x components of each lattice vector were scaled, keeping the fractional coordinates of the nuclei constant. We compressed the unit cell along each direction from $V/V_0=1.00-0.70$ in increments of 0.02, fixing the volume and cell shape at each compression. There were calculations where we were not able to reduce the maximum force on any atom to less than 0.03 eV/Å at a feasible computational expense. These problems occur at high compression due to the large geometrical constraint put on the system. Thus for the calculations with V/V_0 less than 0.86, the maximum force was around 0.05 eV/Å.

III. EQUILIBRIUM PROPERTIES AND HYDROSTATIC COMPRESSION

The unit-cell parameters of HMX were relaxed to find the zero-pressure structure. In Table I, the results of the calculation are compared with the experimental structure at ambient conditions from the data of Eiland and Pepinsky,[30] as well as the results of Choi and Boutin.[31] The lattice vectors $\mathbf{a}_0$, $\mathbf{b}_0$, and $\mathbf{c}_0$ measured by Eiland and Pepinsky using the $P2_1/n$ space group transform[32] into the $P2_1/c$ space group lattice vectors $\mathbf{a}=-\mathbf{a}_0$, $\mathbf{b}=-\mathbf{b}_0$, and $\mathbf{c}=\mathbf{a}_0+\mathbf{b}_0$. Similar to our previous results for PETN,[20] the calculated lattice parameters agree to within 2%–3% of the experimental values. While it is common for the PBE functional to overestimate unit-cell volumes, it has been suggested[7] that the poor description of van der Waals interactions within DFT is responsible for the larger calculated volume.

The unit-cell angles α and γ, just as in experiment, were calculated to be exactly 90.0°, and the calculated angle for β was 0.2° less than the experimental value of 124.3°. The unit cell of β-HMX is shown in Fig. 1.

From the hydrostatic-compression data, the 0 K isotherm was calculated and compared with experiment[2,3] in Fig. 2. Reasonable agreement is shown between our calculations and both of the hydrostatic-compression experiments[2,3] on HMX. Note that the experimental data were collected at room temperature, and we have not corrected the results to account for nonzero temperature. Further, our calculations were performed using the β polymorph of HMX, which is consistent with the experimental data of Gump and Peiris.[3] As observed in previous studies,[20,33] the calculated isotherm appears to approach that of experiment as pressure increases. However, as discussed below, the sample from the experiment of Yoo and Cynn[2] is no longer in the β phase for pressures beyond 12 GPa.

The lattice constants a, b, and c as a function of pressure were also calculated and compared with the experiment[2,3] in Fig. 3. The results are in good agreement until approximately 25 GPa, where the calculated lattice constants begin to differ significantly from the data of Yoo and Cynn.[2] This disagreement is expected because Yoo and Cynn discovered two phase transitions in their hydrostatic-compression experiments,[2] a transition from β to ε at 12 GPa and from ε to ϕ at 27 GPa. Phase transitions are not observed in our calculations because the system is geometrically constrained by using only one elemental unit cell.

To find the bulk modulus and its derivative with respect to pressure, the calculated hydrostatic-compression data up to about 12 GPa were fit to the third-order Birch–Murnaghan (BM) EOS (Ref. 34)

$$P = \tfrac{3}{2}B_0(\eta^{-7/3} - \eta^{-5/3})\left[1 + \tfrac{3}{4}(B_0' - 4)(\eta^{-2/3} - 1)\right], \qquad (1)$$

where $\eta = V/V_0$. In Table II, the values of B_0 and B_0' from this work are compared with experimental values[2,3,35] that are also obtained from fitting to the BM EOS. Poor agreement is shown between different experimental measurements of the bulk modulus. Gump and Peiris[3] have provided data for pressures below 6 GPa, which Menikoff and Sewell[36] have suggested might provide a more accurate value for the bulk modulus via common fitting forms. The underestimation of the bulk modulus from our calculations is expected due to the large overestimation in unit-cell volume at low pressure. Not included in Table II are the results for the bulk modulus and its pressure derivative from various theoretical

TABLE II. Bulk modulus and its derivative with respect to pressure.

Source	Expt./Theory	B (GPa)	B'
Reference 35	Expt.	8.4	26.2
Reference 2	Expt.	16.7	6.8
Reference 3	Expt.	21.0	7.45
This work	Theory	9.8	9.1

TABLE III. Correspondence between indices of the Miller planes in the $P2_1/c$ space group of this work and $P2_1/n$ of Ref. 12.

$P2_1/c$	(100)	(010)	(001)	(110)	(101)	(011)	(111)
$P2_1/n$	(−101)	(0–10)	(001)	(−1−11)	(−102)	(0–11)	(−1−12)

works,[5,6,37] which are tabulated in Ref. 6. Fitting forms other than the BM EOS have been used to calculate these quantities, and the values obtained can vary by as much as 5 GPa (B_0) and 10 (B_0') for the same data set.

IV. UNIAXIAL COMPRESSIONS

The uniaxial compressions have been performed along the directions normal to the low-index Miller planes in the $P2_1/c$ space group shown in Table III, together with the corresponding plane indices in the $P2_1/n$ space group. The principal stresses as a function of compression ratio V/V_0 are shown in Fig. 4. In contrast to the previous work on PETN,[20] the nondiagonal elements of the stress tensor are not zero upon the uniaxial compressions due to the nontrivial shape of the unit cell ($\beta \neq 90°$). Therefore, we calculated the principal stresses by diagonalizing the stress tensor matrix, i.e., by finding its eigenvalues. The principal stresses have been arranged such that σ_1 is the maximum and σ_3 is the minimum. Although the maximum stress in the x direction of compression is not given by the diagonal element of the original stress tensor matrix σ_{xx}, σ_1 is approximately equal to σ_{xx} at small compressions.

The anisotropic behavior of the principal stresses is clearly observed in Fig. 4. The maximum principal stress σ_1 is the greatest for the ⟨011⟩ and ⟨110⟩ compressions. Near $V/V_0=0.82$ there is a decrease in σ_1 in the ⟨011⟩ curve. Note that this corresponds to the compression in the ⟨011⟩ direction where it was difficult to reduce the maximum force below 0.05 eV/Å. Beyond this compression, the greatest value of σ_1 is observed for the ⟨110⟩ compression. The smallest values of σ_1 for uniaxial compression are for the ⟨010⟩ and ⟨001⟩ compressions until about $V/V_0=0.78$, where the ⟨101⟩ compression displays the smallest maximum principal stress. The pressure as a function of V/V_0 from the hydrostatic-compression calculation is included for comparison. The behavior of σ_2 and σ_3 does not show much relative variation between compression directions with the exception of a greater σ_2 for the ⟨001⟩ direction and a lesser σ_3 for the ⟨010⟩ compression.

The change in energy per atom and the band gap as a function of compression are shown in Figs. 5 and 6, respectively. At compressions beyond $V/V_0=0.80$, the greatest change in energy is observed when HMX is compressed in the ⟨110⟩ direction. The ⟨010⟩ and ⟨001⟩ compressions show the least change in energy up to about $V/V_0=0.76$, where the change in curvature of the ⟨101⟩ energy with compression makes it the direction of least energy change. The greatest change in the band gap under compression is observed for the ⟨011⟩ compression (by −0.85 eV). The ⟨101⟩ and ⟨001⟩ compressions show a very little change in the band gap with compression in comparison to the results from other directions. There have been theoretical investigations suggesting that the reduction in the band gap as a result of compression

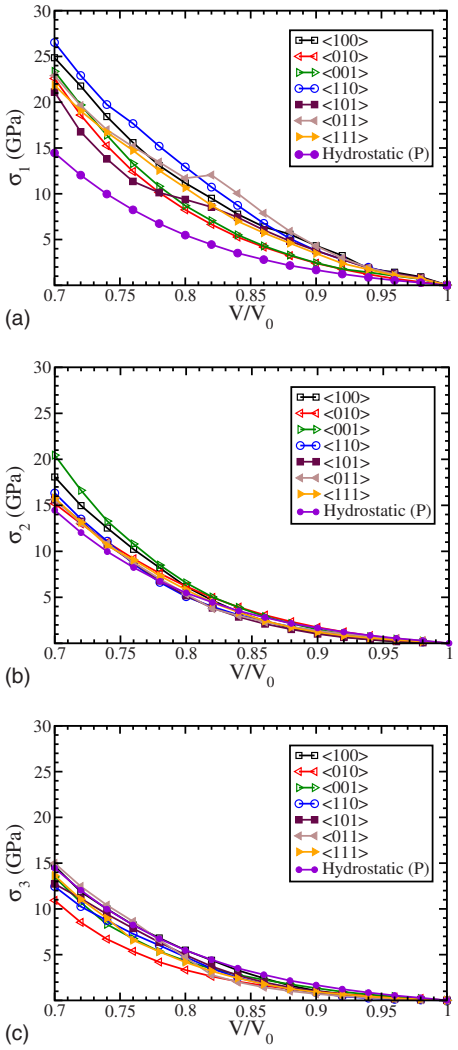

FIG. 4. (Color online) Principal stresses as a function of V/V_0. The pressure from the hydrostatic-compression calculations is shown for comparison.

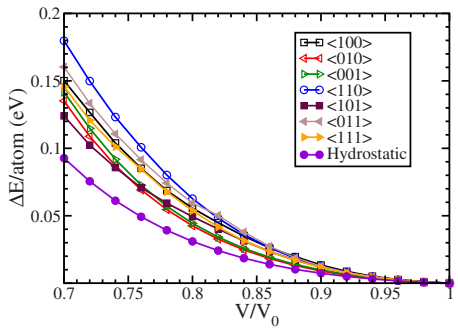

FIG. 5. (Color online) Change in energy per atom as a function of compression.

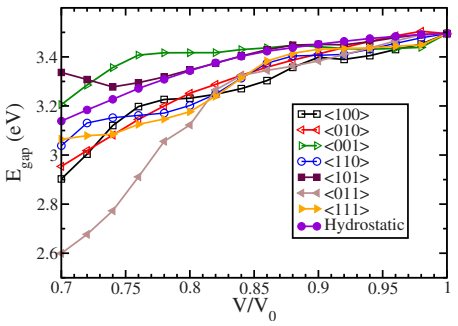

FIG. 6. (Color online) Band gap as a function of compression.

may influence the sensitivity of an EM,[38,39] but in the case of β-HMX we have not observed a substantial reduction in the band gap toward zero.

The shear stresses as a function of compression for each direction are shown in Fig. 7. The shear stresses were calculated as

$$\tau = \frac{\sigma_i - \sigma_j}{2}, \tag{2}$$

where $i \neq j$ takes the values 1, 2, and 3. The maximum shear stress $\tau_{\max}$ is found by using $i=1$ and $j=3$, but the values of i and j used to find τ_{mid} and $\tau_{\min}$ depend on the principal stresses for the given compression direction.

The $\langle 011 \rangle$ compression shows the greatest shear stress under compression up to around $V/V_0=0.84$, which is also the first structure where relaxing the forces in the structure below 0.04 eV/Å became difficult. Meanwhile, the $\langle 110 \rangle$ compression shows relatively large values for $\tau_{\max}$ and τ_{mid}. On the other hand, these shear stresses are small for the $\langle 010 \rangle$ and $\langle 001 \rangle$ compressions. At higher compression, the $\langle 101 \rangle$ direction has the smallest values of $\tau_{\max}$ and τ_{mid}. Further, both the $\langle 101 \rangle$ and $\langle 011 \rangle$ compressions show a nonmonotonic dependence of shear stress upon strain.

The experimental work on the uniaxial compression of HMX performed by Dick *et al.*[12] was done using the directions specified in the $P2_1/n$ space group. However, our calculations were done using the standard space group $P2_1/c$ prior to our knowledge of their experiments. A full comparison of our calculations with the experimental shock wave profiles is not possible without recalculating the uniaxial compressions along the crystallographic directions defined according to the $P2_1/n$ space group.

V. CONCLUSIONS

Hydrostatic and uniaxial compressions in directions normal to the {100}, {010}, {001}, {110}, {101}, {011}, and {111} planes were performed using the first-principles DFT code VASP with the PBE functional and PAW potentials. The calculated zero-pressure structure was compared with the experimental structure at ambient conditions, and the lattice parameters agree to within 2%–3%. The hydrostatic-compression data were used to calculate the 0 K isotherm, which showed reasonable agreement with the experimental data at room temperature.

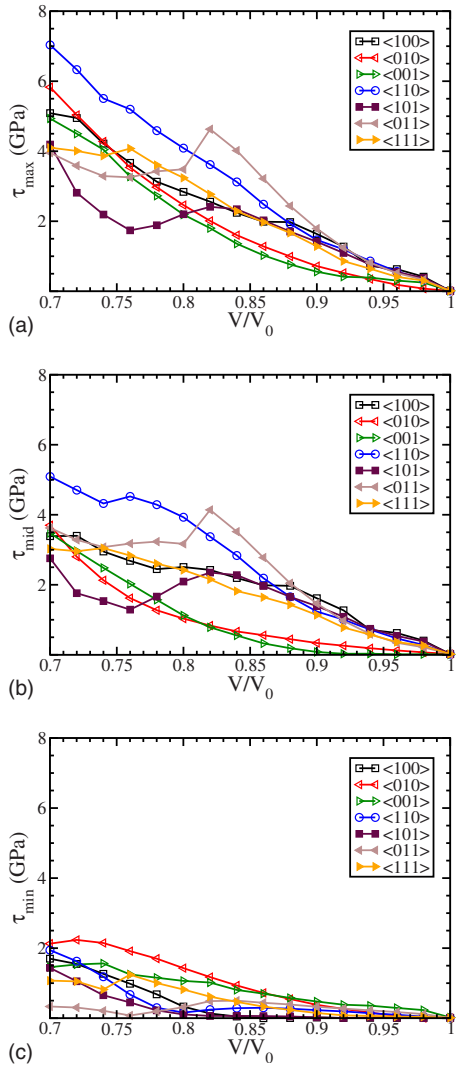

FIG. 7. (Color online) Shear stresses as a function of V/V_0.

The energy per atom, band gap, principal stresses, and shear stresses as functions of V/V_0 were calculated. The results indicate anisotropic behavior of these physical quantities under compression. In the previous work on PETN,[20] the shear stresses were compared with the experimental data regarding sensitivity to examine the possibility of a correlation. For HMX, no known experimental data regarding anisotropic sensitivity exist. Further, the available experiments on uniaxial compression of HMX (Ref. 12) were performed using a different space group from the one used in the calculations presented in this paper. In the future, we will perform calculations using the space group and compression directions used in these experiments in an attempt to correlate the shear stress behavior and shock sensitivities along specific crystallographic directions.

ACKNOWLEDGMENTS

The authors wish to thank D. Hooks, M. Nicol, S. Peiris, and O. Tschauner for stimulating discussions. The work at USF was supported by the Office of Naval Research (ONR) through the Naval Research Laboratory (NRL) (Grant Nos. N00173-06-1-G022 and N00173-08-2-C002) and partly by

the Army Research Office through the Multi-University Research Initiative on Insensitive Munitions (Grant No. W901NF-05-1-0266) and DURIP (Grant No. W911NF-07-1-0212). The work at Caltech was supported by the Office of Naval Research (ONR) (Grant No. N00014-05-1-0778) and the Army Research Office through the Multi-University Research Initiative on Insensitive Munitions (Grant No. W911NF-05-1-0345). The work at NRL was supported by ONR both directly (Grant No. N00014-08-WX-20138) and through NRL. The computations were performed using NSF Teragrid computational facilities (Grant No. TG-DMR070018N).

[1]H. H. Cady and L. C. Smith, LANL Report No. LAMS-2652, 3 May 1962.
[2]C. S. Yoo and H. Cynn, J. Chem. Phys. **111**, 10229 (1999).
[3]J. C. Gump and S. M. Peiris, J. Appl. Phys. **97**, 053513 (2005).
[4]T. D. Sewell, J. Appl. Phys. **83**, 4142 (1998).
[5]D. C. Sorescu, B. M. Rice, and D. L. Thompson, J. Phys. Chem. B **103**, 6783 (1999).
[6]T. D. Sewell, R. Menikoff, D. Bedrov, and G. D. Smith, J. Chem. Phys. **119**, 7417 (2003).
[7]E. F. C. Byrd, G. E. Scuseria, and C. F. Chabalowski, J. Phys. Chem. B **108**, 13100 (2004).
[8]E. F. C. Byrd and B. M. Rice, J. Phys. Chem. C **111**, 2787 (2007).
[9]W. Zhu, J. Xiao, G. Ji, F. Zhao, and H. Xiao, J. Phys. Chem. B **111**, 12715 (2007).
[10]L. Dan, L. Lai-Yu, W. Dong-Qing, Z. Qing-Ming, G. Zi-Zheng, and G. Yong-Xin, Chin. Phys. Lett. **25**, 899 (2008).
[11]F. J. Zerilli and M. M. Kuklja, J. Phys. Chem. A **110**, 5173 (2006).
[12]J. J. Dick, D. E. Hooks, R. Menikoff, and A. R. Martinez, J. Appl. Phys. **96**, 374 (2004).
[13]J. J. Dick and J. P. Ritchie, J. Appl. Phys. **76**, 2726 (1994).
[14]J. J. Dick, J. Appl. Phys. **81**, 601 (1997).
[15]R. Menikoff, J. J. Dick, and D. E. Hooks, J. Appl. Phys. **97**, 023529 (2005).
[16]D. E. Hare, J. W. Forbes, D. B. Reisman, and J. J. Dick, Appl. Phys. Lett. **85**, 949 (2004).
[17]D. E. Hooks, D. B. Hayes, D. E. Hare, D. B. Reisman, K. S. Vandersall, J. W. Forbes, and C. A. Hall, J. Appl. Phys. **99**, 124901 (2006).
[18]P. J. Rae, D. E. Hooks, and C. Liu, in Proceedings of the 13th International Detonation Symposium, edited by S. M. Peiris (Office of Naval Research, Norfolk, VA, 2006), p. 293.
[19]D. E. Hooks and K. J. Ramos, in Proceedings of the 13th International Detonation Symposium, edited by S. M. Peiris (Office of Naval Research, Norfolk, VA, 2006), p. 455.
[20]M. W. Conroy, I. I. Oleynik, S. V. Zybin, and C. T. White, Phys. Rev. B **77**, 094107 (2008).
[21]P. Hohenberg and W. Kohn, Phys. Rev. **136**, B864 (1964); W. Kohn and L. J. Sham, *ibid.* **140**, A1133 (1965).
[22]G. Kresse and J. Furthmuller, Phys. Rev. B **54**, 11169 (1996).
[23]G. Kresse and J. Furthmuller, Comput. Mater. Sci. **6**, 15 (1996).
[24]J. P. Perdew, K. Burke, and M. Ernzerhof, Phys. Rev. Lett. **77**, 3865 (1996).
[25]J. P. Perdew, K. Burke, and M. Ernzerhof, Phys. Rev. Lett. **78**, 1396 (1997).
[26]P. E. Blochl, Phys. Rev. B **50**, 17953 (1994).
[27]G. Kresse and D. Joubert, Phys. Rev. B **59**, 1758 (1999).
[28]H. J. Monkhorst and J. D. Pack, Phys. Rev. B **13**, 5188 (1976).
[29]J. J. Dick, R. N. Mulford, W. J. Spencer, D. R. Pettit, E. Garcia, and D. C. Shaw, J. Appl. Phys. **70**, 3572 (1991).
[30]P. R. Eiland and R. Pepinsky, Z. Kristallogr. **106**, 273 (1955).
[31]C. S. Choi and H. P. Boutin, Acta Crystallogr., Sect. B: Struct. Crystallogr. Cryst. Chem. **26**, 1235 (1970).
[32]H. H. Cady, A. C. Larson, and D. T. Cromer, Acta Crystallogr. **16**, 617 (1963).
[33]H. Liu, J. J. Zhao, D. Q. Wei, and Z. Z. Gong, J. Chem. Phys. **124**, 124501 (2006).
[34]C. K. Gan, T. D. Sewell, and M. Challacombe, Phys. Rev. B **69**, 035116 (2004).
[35]B. Olinger, B. Roof, and H. Cady, Proceedings of the International Symposium on High Dynamic Pressures (C.E.A., Paris, 1978), pp. 3–8.
[36]R. Menikoff and T. Sewell, High Press. Res. **21**, 121 (2001).
[37]J. P. Lewis, T. D. Sewell, R. B. Evans, and G. A. Voth, J. Phys. Chem. B **104**, 1009 (2000).
[38]M. M. Kuklja, E. V. Stefanovich, and A. B. Kunz, J. Chem. Phys. **112**, 3417 (2000).
[39]M. M. Kuklja, B. P. Aduev, E. D. Aluker, V. I. Krasheninin, A. G. Krechetov, and A. Y. Mitrofanov, J. Appl. Phys. **89**, 4156 (2001).